JOURNAL OF MATERIALS SCIENCE 33 (1998) 681–686

Failure mechanism of a thermal barrier coating system on a nickel-base superalloy

H. M. TAWANCY, N. SRIDHAR, N. M. ABBAS
Materials Characterization Laboratory, Metrology, Standards and Materials Division, Research Institute, King Fahd University of Petroleum and Minerals, P.O. Box 1639, Dhahran 31261, Saudi Arabia

D. RICKERBY
Rolls-Royce plc, Derby DW24 8BJ, UK

An investigation was carried out to determine the failure mechanism of a thermal barrier coating system on an Ni-base superalloy. The coating system consisted of an outer layer of yttria-stabilized zirconia (top coat), and an inner layer of Pt-aluminide (bond coat). Specimens were exposed at 1010 and 1150 °C with a 24-h cycling period to room temperature. Scanning electron microscopy combined with energy dispersive X-ray spectroscopy as well as X-ray diffraction were used in microstructural characterization. Spallation of the oxide scale developed by the bond coat was found to be the mode of failure. Experimental results indicated that the breakdown of oxide was affected by internal oxidation of Hf diffusing from the alloy substrate into the bond coat surface developing localized high levels of stress concentration at the oxide–bond coat interface. It was concluded that the cause of failure was degradation of thermal stability of the bond coat accelerating its oxidation rate and permitting outward diffusional transport of elements from the substrate.

1. Introduction

To achieve greater efficiencies and higher thrusts of aircraft gas turbine engines, increased demands are imposed on the structural materials of turbine components [1]. In particular, significant reductions in fuel consumption can only be achieved by increasing the gas temperature at the inlet throat of the turbine section, requiring the use of materials with greater temperature capabilities [2]. Improved cooling methods and use of thermal barrier coatings are considered to be the most technically and economically feasible means for increasing the operating temperature of a gas turbine engine [3].

Typically, a thermal barrier coating (TBC) system consists of an outer ceramic coating (top coat layer), usually yttria-stabilized zirconia, glued to an inner metallic coating layer (bond coat) by means of a thin layer of Al_2O_3 [4]. It is the function of the top ceramic coat to act as a thermal insulator. Adhesion of the top coat to the bond coat is the key to successful applications of TBC systems in protecting rotating parts of gas turbine engines. Previous work had demonstrated that the useful life of a TBC system is to a large extent governed by the oxidation properties of the bond coat [5–9]. It was the objective of this study to determine the failure mechanism of a TBC system on a Ni-base superalloy with particular emphasis on the oxidation properties of the bond coat.

2. Experimental procedure

Table I summarizes the nominal chemical composition of the alloy substrate. Rods of the alloy about 8 mm in diameter were first platinum aluminized to produce a Pt–aluminide coating containing a nominal of 55 wt % Pt and 25 wt % Al. Subsequently, the top coat was applied by the electron beam vacuum evaporation technique [4]. Specimens about 10 mm in length were exposed at 1010 and 1150 °C and cycled to room temperature every 24 h (air cooling) until failure occurred as indicated by spallation of the top coat. To characterize the interfacial oxide layer, specimens were deep etched in a solution consisting of 10% bromine and 90% methanol by volume. Scanning electron microscopy (SEM) combined with energy dispersive X-ray spectroscopy capable of detecting light elements, and X-ray diffraction were used in microstructural characterization. To characterize the oxide layer near the oxide–bond coat interface in the SEM, specimens were tilted about 60°.

3. Results and discussion

3.1. Coating microstructure in the heat-treated condition

Characteristic microstructural features of the coating system in the heat-treated condition are summarized in Fig. 1. It is observed from Fig. 1a that the ceramic

TABLE I Nominal chemical composition of the alloy substrate (wt %)

Ni	Cr	Al	Ti	Co	W	Ta	Mo	Hf	Fe	Zr	B	C
Bal.	9	5.5	1.5	10	10	2.5	0.5*	1.25	0.5*	0.055	0.015	0.015

* Maximum.

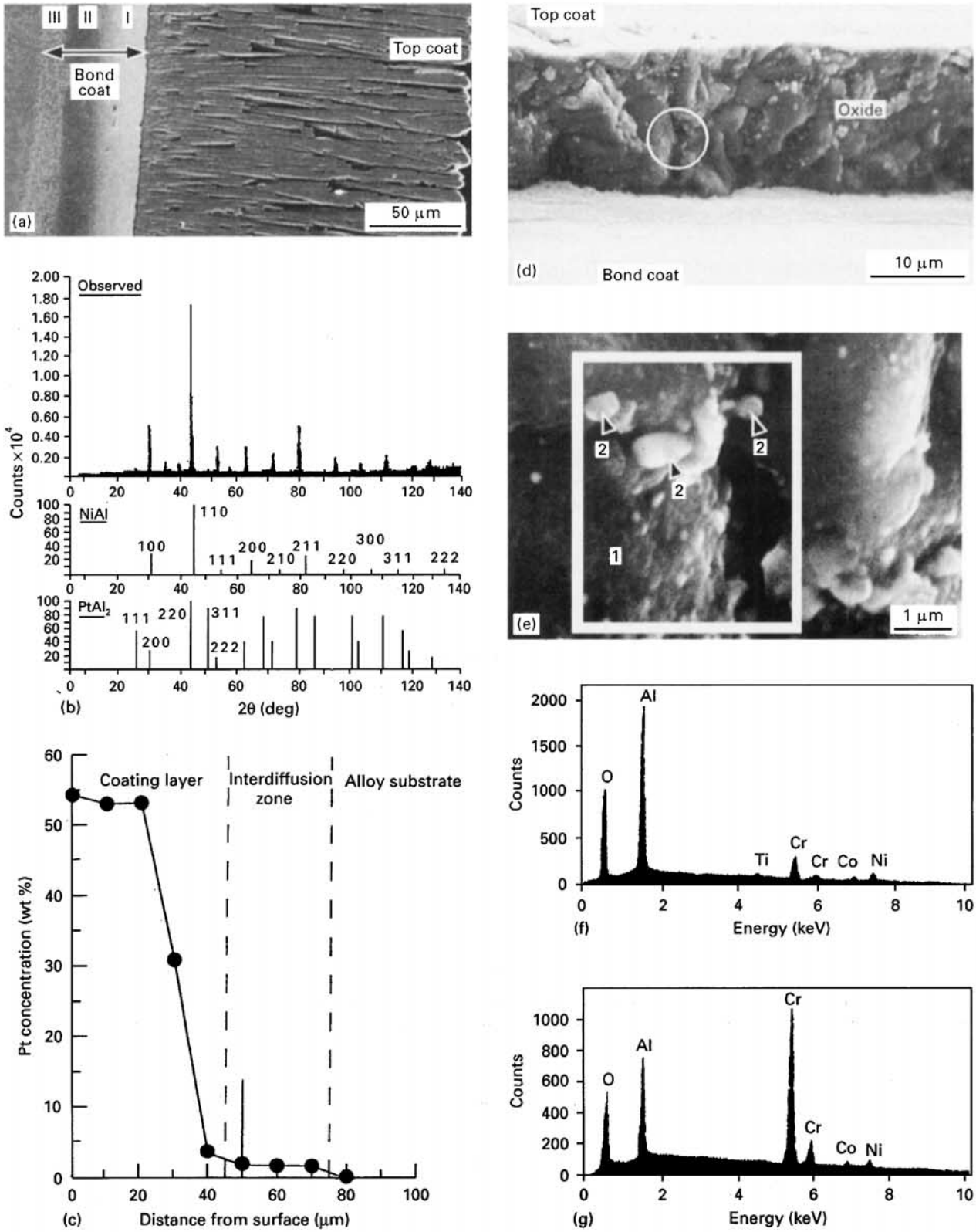

Figure 1 Characteristic microstructural features of the coating system in the heat-treated condition: (a) is a secondary-electron SEM image illustrating the coating morphology (0° tilt), (b) is an X-ray diffraction pattern derived from the bond coat surface in comparison with standard patterns of NiAl and $PtAl_2$, (c) is a concentration profile of Pt across the bond coat and into the substrate, (d) and (e) are secondary electron SEM images illustrating the morphology of the interfacial oxide layer (60° tilt), and (f) and (g) are energy dispersive X-ray spectra derived from Regions 1 and 2 in (e), respectively.

top coat had a thickness of about 200 μm, and it consisted of dense columnar grains typically produced by the electron beam vacuum evaporation technique [4]. Fig. 1a also shows that the bond coat consisted of three distinct zones:

1. an outer zone about 20 μm in thickness (zone I),
2. an intermediate zone about 15 μm in thickness (zone II), and
3. an inner interdiffusion zone about 15 μm in thickness (zone III).

Most of the Pt in the bond coat was present within the 20 μm surface layer (zone I), which consisted of $PtAl_2$ dispersed in a matrix of β-phase (NiAl + Cr, Co, Pt and Ti in solid solution) as shown in Fig. 1b and c [10]. Zone II was found to consist of Ni-rich β-phase, and zone III consisted of σ-phase and material composite (MC)-type carbides dispersed in a β-phase matrix. Analysis of the interfacial oxide layer bonding the top coat to the bond coat showed that it consisted of Cr-rich oxide particles dispersed in a matrix of Al_2O_3 as illustrated in Fig. 1d–f.

3.2. Oxidation behaviour of the bond coat

Fig. 2 illustrates the effect of exposure time at 1010 and 1150 °C on the thicknesses of the thermally grown oxides. After an initial stage of rapid oxidation kinetics, parabolic rate behaviour was followed at both temperatures. However, this was interrupted by breakaway oxidation after about 120 h exposure at 1150 °C, indicating that the scale became non-protective and suggesting that a direct correlation existed between the oxide thickening rate and time to failure. At both temperatures, the oxidation reaction proceeded by growth of an Al_2O_3 layer containing Cr-rich oxide particles, however, Hf-rich oxide particles were also developed within the scale. Evidently, during thermal exposure, Hf had diffused from the alloy substrate into the surface of the bond and then was incorporated into the oxide as Hf-rich oxide particles. Both the morphologies and compositions of the oxides developed at 1010 and 1150 °C were similar, however, the Hf-rich oxide particles developed at 1150 °C were comparatively coarser reflecting an increased extent of outward diffusional transport of Hf.

As an example, Fig. 3 illustrates the effect of exposure time at 1150 °C on the oxide morphology and composition prior to failure. It is observed that the Hf-rich oxide particles assumed a peg-type

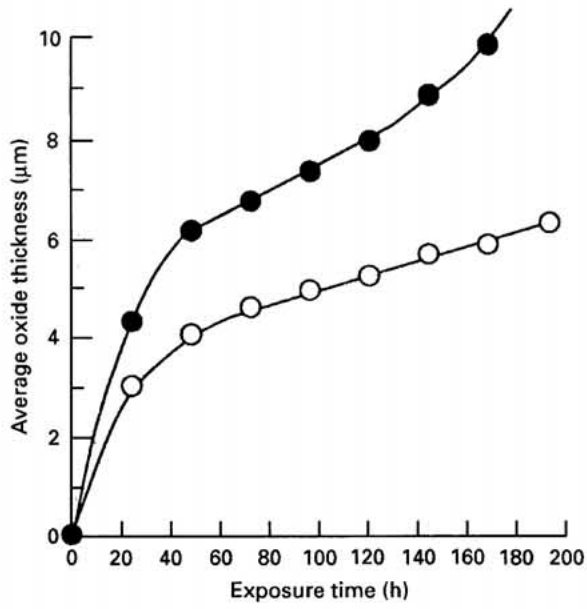

Figure 2 Effect of exposure time at (○) 1010 °C and (●) 1150 °C on the thicknesses of thermally grown oxides.

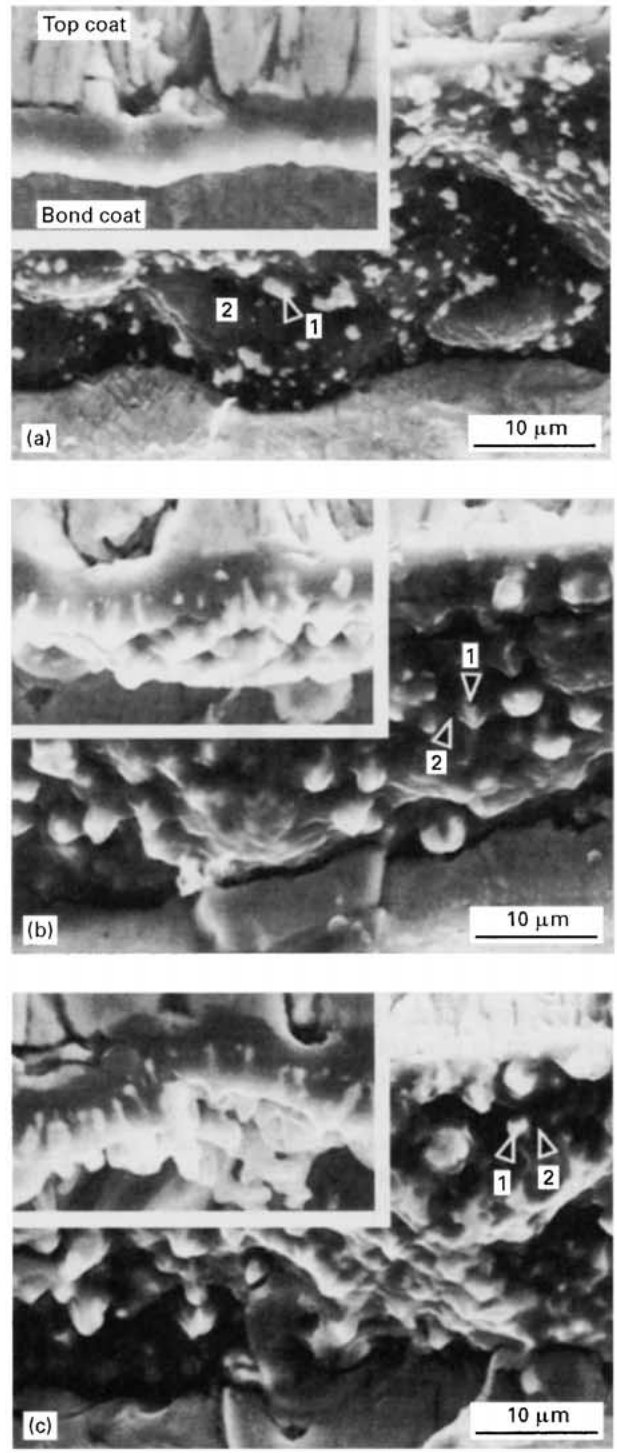

Figure 3 Effect of exposure time at 1150 °C on the oxide morphology and composition. (a), (b) and (c) are secondary electron SEM images illustrating the morphology of the oxide after 24, 48 and 72 h exposure as viewed at 60° tilt (the insets show the respective morphology at 0° tilt); and (d) and (e) are X-ray spectra derived from Regions 1 and 2 in (a), (b) and (c).

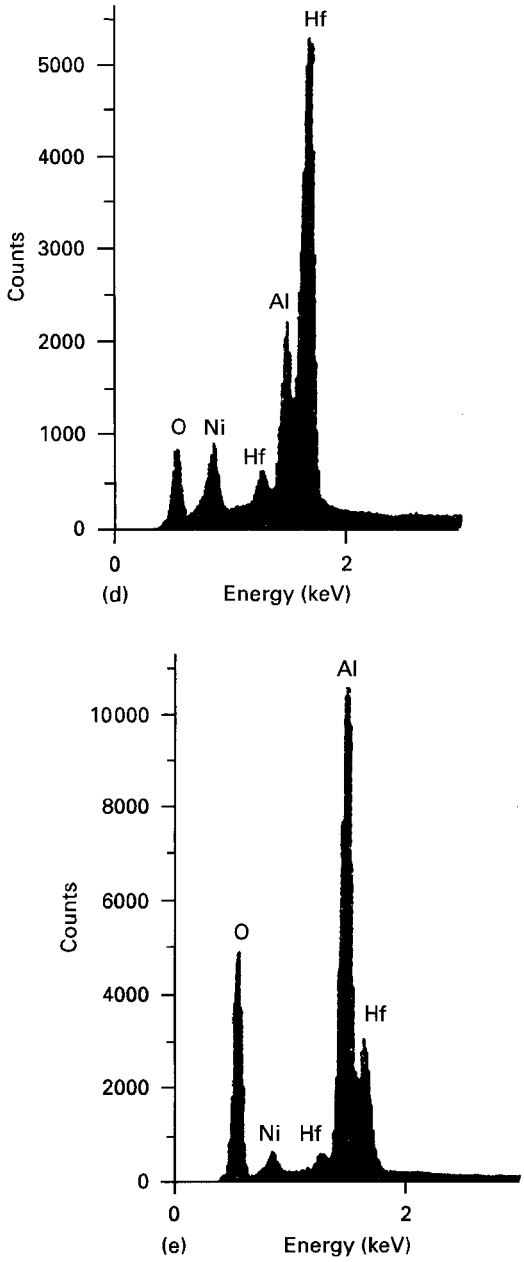

Figure 3 (Continued).

morphology and were enveloped by Al_2O_3, which appeared to penetrate the bond coat indicating that Hf was internally oxidized by inward diffusion of oxygen. It is to be noted that relatively large oxide pegs enriched in active elements such as Hf were reported to degrade the adherence of Al_2O_3, which could be related to localized high levels of stress concentration at the oxide–substrate (bond coat in this case) interface [11].

3.3. Thermal stability of the bond coat

Fig. 4 shows the effect of exposure time at 1150 °C on the average Pt concentration in the outermost coating layers. It is observed that after 24 h exposure at 1150 °C, the Pt concentration is reduced from about 55 wt % to 20 wt %. However, there is no significant change in Pt concentration with continued exposure. Corresponding to the above reduction in Pt concentration, the constituents of the bond coat appear to

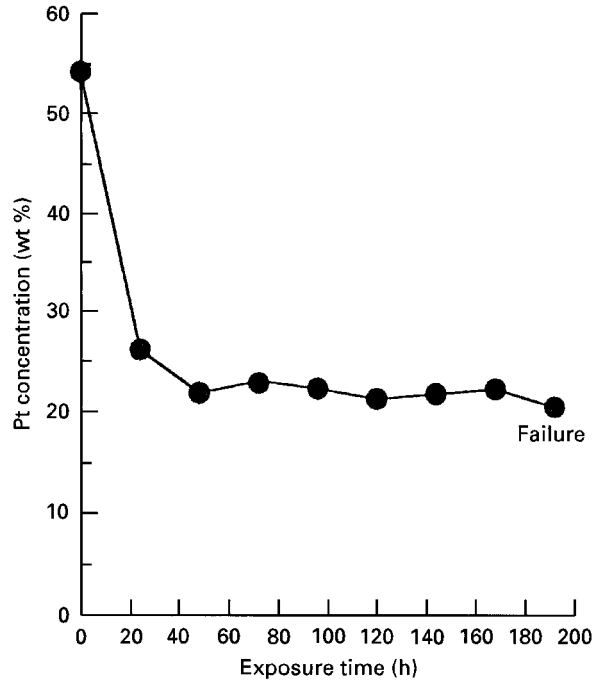

Figure 4 Effect of exposure time at 1150 °C on the average Pt concentration in the outermost coating layer.

change from a mixture of $PtAl_2$ and β-phase into a mixture of β-phase and γ′-phase containing Pt in solid solution as illustrated in Fig. 5 and Table II. Evidently, as a result of interdiffusion and the corresponding change in the relative concentrations of Ni, Pt and Al, $PtAl_2$ became thermodynamically unstable.

3.4. Failure behaviour

After up to 2856 h exposure (119 cycles) at 1010 °C, the top coat remained to be adhered to the bond coat. In contrast, failure occurred after 192 h exposure (eight cycles) at 1150 °C. However, in this case, the top coat was observed to lose its adherence to the bond coat only during cooling and particularly as room temperature was approached. This observation suggested that the stresses developed during isothermal exposure were relieved by diffusion-controlled deformation [12–14], however, the continued build-up of thermal stresses during cooling could lead to failure.

Fig. 6 illustrates characteristic microstructural features of the bond coat surface after failure at 1150 °C (192 h exposure). It is observed from Fig. 6a that the surface morphology resembles a fracture surface produced by microvoid coalescence resulting in dimples containing second-phase particles. Microchemical analysis (Table III) of the indicated regions in Fig. 6b shows that the dimple-like regions consist of Al_2O_3 enveloping particles of a Hf-rich oxide as illustrated in the X-ray spectra of Fig. 6c and d, respectively. As shown in Fig. 6e, the Al concentration of the bond coat approaches that of Ni suggesting that it consists of β-phase, however, X-ray diffraction analysis shows that a γ′-phase is also present (Fig. 6f) consistent with the results of Fig. 5. As shown in Fig. 6f, the oxide phases are identified as α-Al_2O_3 and HfO_2. Fig. 7

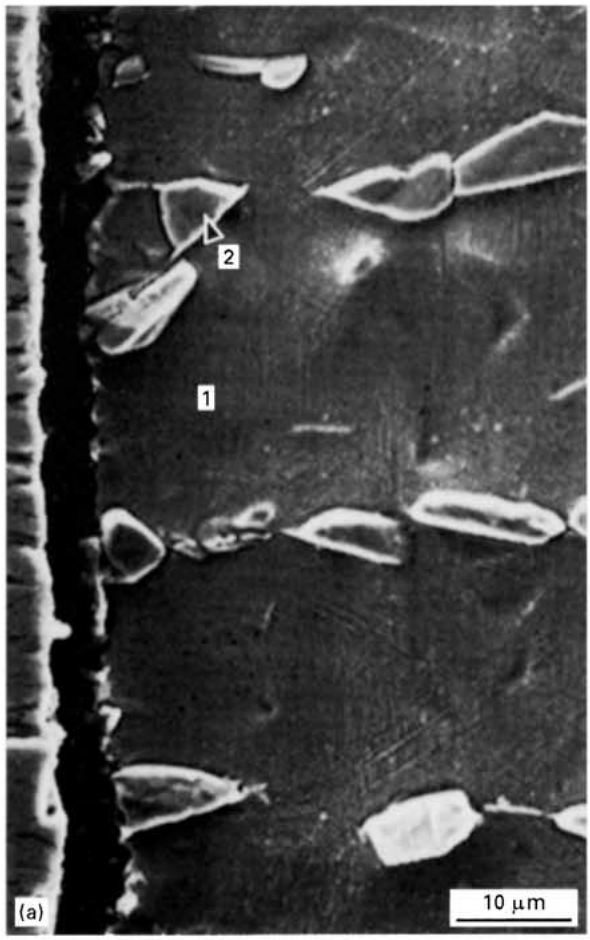

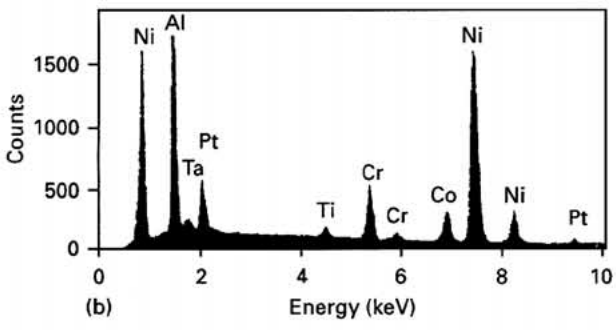

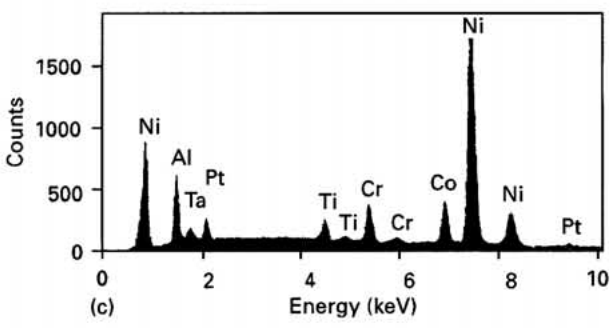

Figure 5 Morphology and composition of the bond coat after 72 h exposure at 1150 °C. (a) is a secondary electron SEM image, and (b) and (c) are energy dispersive X-ray spectra.

TABLE II Quantified spectral data results from Regions 1 and 2 in Fig. 5a (at %)

	Ni	Al	Pt	Co	Cr	Ta	Ti
Region 1	44.92	34.61	6.26	4.75	7.79	0.55	1.12
Region 2	60.87	19.11	2.73	7.45	6.18	1.21	2.45

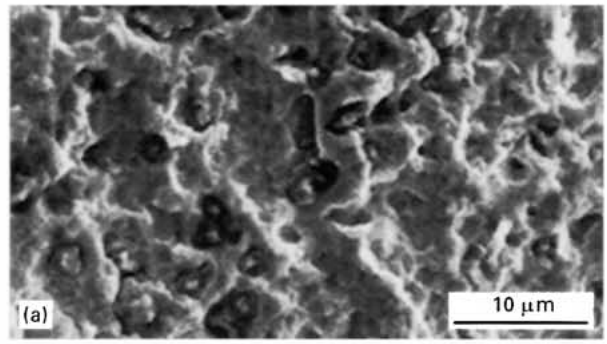

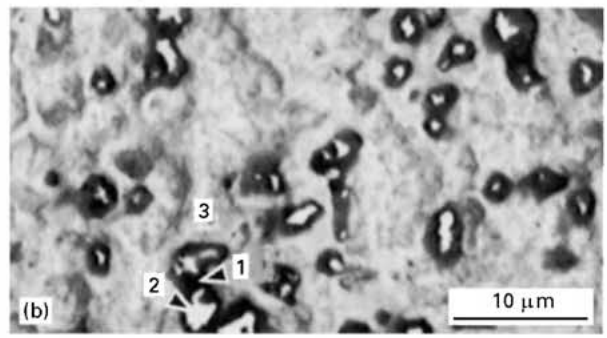

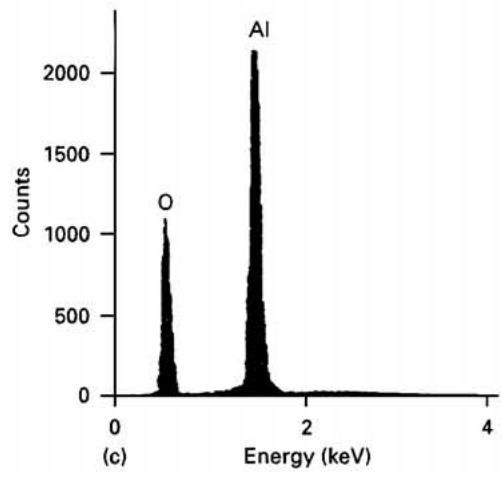

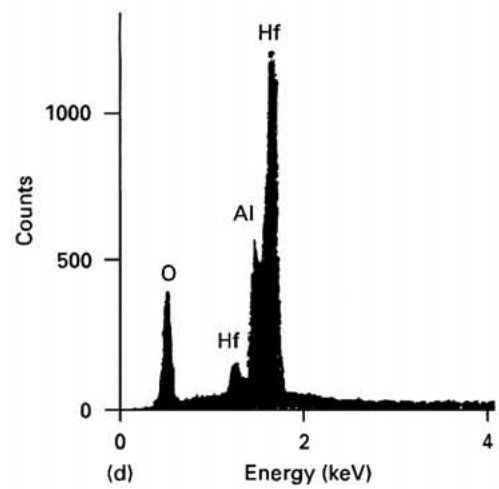

Figure 6 Microstructure of the bond coat surface after failure (192 h at 1150 °C). (a) and (b) are secondary and backscattered composition images of the same region; (c), (d), and (e) are X-ray spectra derived from Regions 1, 2 and 3 in (b), respectively; and (f) is the corresponding X-ray diffraction pattern.

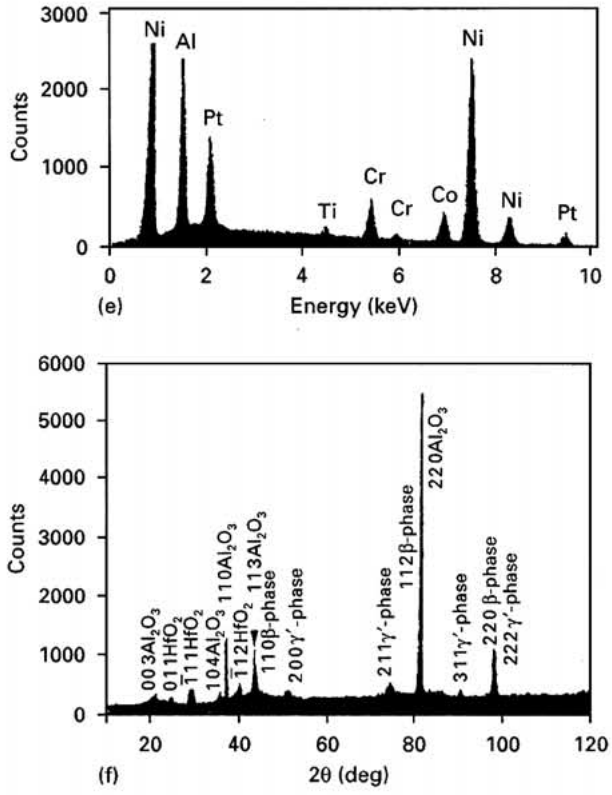

Figure 6 (Continued).

TABLE III Microchemical analysis (at %) of the dimple-like regions shown in Fig. 6b

Ni	Co	Cr	Pt	Al	Ti
49.81	6.59	6.03	5.80	30.67	1.10

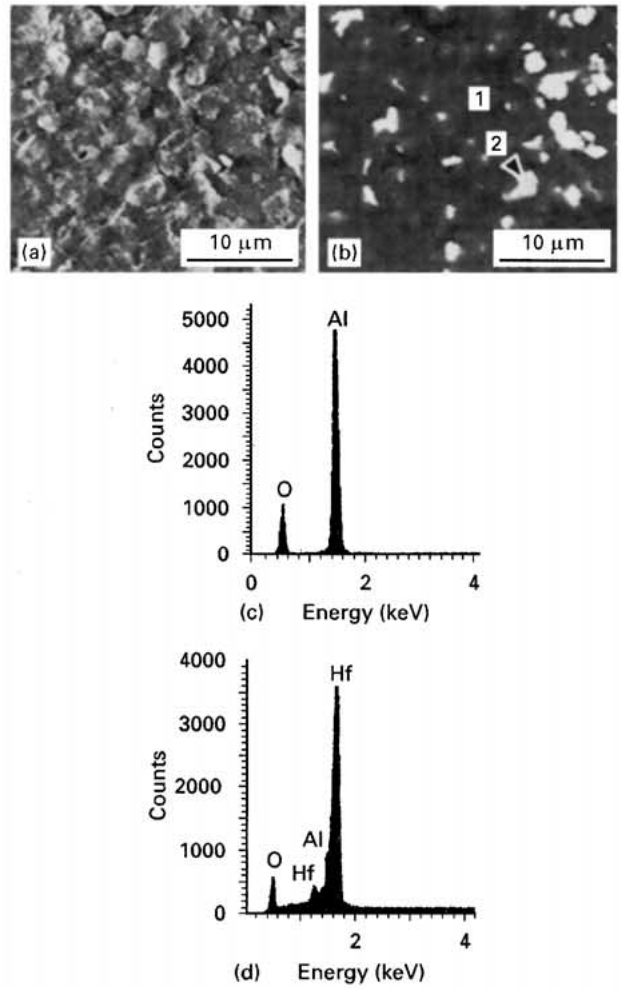

Figure 7 Microstructure of the bottom surface of the top coat after failure (192 h at 1150 °C). (a) and (b) are secondary and backscattered composition images of the same region, respectively; and (c) and (d) are X-ray spectra derived from Regions 1 and 2 in (b), respectively.

shows that the bottom surface of the top coat is covered by Al_2O_3 indicating that the mode of failure is spallation of the oxide developed by the bond coat. Evidently, oxide spallation was the most favourable mode of accommodating the high localized levels of stress developed as a result of the differences in thermal expansion–contraction characteristics of the oxide and bond coat particularly at those regions of the oxide–bond coat interface where internal oxidation of Hf occurred leading to the development of oxide pegs.

4. Conclusions

Oxide spallation was found to be the mode of failure of a thermal barrier coating system on an Ni-base superalloy containing Hf. Most evidence pointed out that the driving force for spallation was provided by the continued build-up of thermal stresses during cooling particularly at those regions of the oxide–bond coat interface where internal oxidation of Hf had occurred. Degradation of thermal stability of the bond coat accelerating its oxidation rate and permitting the outward diffusional transport of elements from the alloy substrate could be identified as the cause of failure.

References

1. D. DRIVE, in "Materials at their limit" (The Institute of Metals, London, 1984) p. 63.
2. G. L. WILDE, *J. Aerospace Engng* **209** (1995) 85.
3. C. T. SIMS, *Adv. Mater. Processes* **139** (1991) 32.
4. H. LÄMMERMANN and G. KIENEL, *ibid.* **140** (1991) 18.
5. U. DIETL, *Surf. Coatings Technol.* **68/69** (1994) 17.
6. J. H. SUN, E. CHANG, C. H. CHAO and M. CHENG, *Oxid. Metall.* **40** (1993) 465.
7. S. M. MEIER, D. M. NISSLEY, K. D. SHEFFLER and T. A. CRUSE, *Trans. ASME* **114** (1992) 258.
8. W. LIH, E. CHANG, B. C. WU and C. H. CHAO, *Oxid. Metall.* **36** (1991) 221.
9. R. A. MILER, *J. Engng Gas Turbines & Power* **111** (1989) 301.
10. H. M. TAWANCY, N. SRIDHAR, N. M. ABBAS and D. RICKERBY, *Scripta Metall. Mater.* **33** (1995) 1431.
11. D. DELAUNAY and A. M. HUNTZ, *J. Mater. Sci.* **17** (1982) 2027.
12. J. JEDLINSKI, *Solid-State Phenomena* **21/22** (1992) 335.
13. F. H. STOTT, in "The role of active elements in the oxidation behavior of high-temperature metals and alloys", edited by E. Lang (Elsevier, London, 1989) p. 3.
14. J. R. NICHOLLS and P. HANCOCK in "The role of active elements in the oxidation behaviour of high-temperature metals and alloys", edited by E. Lang (Elsevier, London, 1989) p. 195.

Received 18 Septemper 1996
and accepted 17 June 1997